GEOPHYSICS, VOL. 69, NO. 1 (JANUARY-FEBRUARY 2004); P. 78–86, 11 FIGS., 3 TABLES.
10.1190/1.1649377

Inversion of magnetotelluric data for 2D structure with sharp resistivity contrasts

Catherine de Groot-Hedlin* and Steven Constable*

ABSTRACT

We have developed a linearized algorithm to invert noisy 2-D magnetotelluric data for subsurface conductivity structures represented by smooth boundaries defining sharp resistivity contrasts. We solve for both a fixed number of subsurface resistivities and for the boundary locations between adjacent units. The boundary depths are forced to be discrete values defined by the mesh used in the forward modeling code. The algorithm employs a Lagrange multiplier approach in a manner similar to the widely used Occam method. The main difference is that we penalize variations in the boundary depths, rather than in resistivity contrasts between a large number of adjacent blocks. To reduce instabilities resulting from the breakdown of the linear approximation, we allow an option to penalize contrasts in the resistivities of adjacent units.

We compare this boundary inversion method to the smooth Occam inversion for two synthetic models, one that includes a conductive wedge between two resistors and another that includes a resistive wedge between two conductors. The two methods give good agreement for the conductive wedge, but the solutions differ for the more poorly resolved resistive wedge, with the boundary inversion method giving a more geologically realistic result. Application of the boundary inversion method to the resistive Gemini subsalt petroleum prospect in the Gulf of Mexico indicates that the shape of this salt feature is accurately imaged by this method, and that the method remains stable when applied to real data.

INTRODUCTION

Since any real magnetotelluric (MT) data set consists of a finite number of imprecise data values, the nonlinear geophysical inverse problem of finding a model with a response that fits the data is ill-posed, and there are an infinite number of models that fit the data equally well above some threshold misfit (below which no models can be found). The task of model construction thus entails introducing a selection criterion to narrow the search down to a class of model having some preferred characteristics. Two-dimensional (2D) MT inverse methods may be categorized in terms of the selection criteria used to choose from this infinite set of models.

Parameterized inversion methods (e.g., Jupp and Vozoff, 1977; Oristaglio andWorthington, 1980) follow the strategy of finding a model that is close to some "ideal" form. Interpretations based on this method involve constructing a cross-section of the MT transect based on prior geological knowledge, and computing conductivities through least squares inversion. These methods are highly dependent on model parameterization and on the accuracy and availability of the prior geological information.

Another option is to overparameterize the problem, that is, break the model into more parameters than there are data, and constrain the inversion through a regularization method (Tihonov, 1963a, b). Regularization involves simultaneously minimizing the data misfit as well as some other undesirable feature of the model. A now standard approach is to find the smoothest model that fits the data. Various methods of defining model smoothness may be found in Rodi (1989), de Groot-Hedlin and Constable (1990), Smith and Booker (1991), Uchida (1993), and Rodi and Mackie (2001). Imposition of the smoothness constraint stabilizes the inversion algorithm and avoids the introduction of anomalous conductivities that are simply artifacts of the inversion method. However, models derived by these methods may be geologically unrealistic in situations in which it is known (from well-log information, for instance) that the subsurface structure consists of geological formations of nearly uniform conductivity separated by sharp boundaries. This is often the case in petroleum exploration targets in which the MT method is applied (e.g., Hoversten et al., 2000).

Given that the MT method involves the measurement of relatively low-frequency, diffusive electromagnetic (EM) fields,

Manuscript received by the Editor November 27, 2002; revised manuscript received July 29, 2003.
*University of California at San Diego, Scripps Institute of Oceanography, 8775 Biological Grade, La Jolla, California 92093-0225. E-mail: chedlin@ucsd.edu; sconstable@ucsd.edu.

it is not ideally suited to defining boundaries. However, in situations where it is known a priori that the substrate consists of geological units with sharp resistivity contrasts, MT inversion methods that allow for blocky structures are useful. One approach, developed by Mehanee and Zhdanov (2002), is to minimize the total area of the anomalous model parameters. Another approach is to solve for boundary locations directly. Several such algorithms have been developed: Marcuello-Pascuel et al. (1992) present a method in which conductivity values are held fixed while solving for the boundaries, which may be represented by one of several simple geometrical functions. Smith et al. (1999) describe an algorithm to solve simultaneously for smoothly-varying boundary depths between geological units, as well as laterally smoothly-varying conductivities within each unit.

One difficulty with a linearized MT inversion for models with sharp resistivity contrasts is that the linearity assumption breaks down with increasing resistivity contrast between units (e.g., Smith et al., 1999). A breakdown in the linearity assumption can yield instability in a linearized inversion routine. In this paper, we present a robust algorithm to invert noisy 2D MT data for conductivity structures represented by a limited number of layers of uniform resistivity and laterally variable thickness. We ensure stability by introducing an option to penalize resistivity constrasts between adjacent layers. Details of the algorithm are presented in the next section. In the following sections, we apply the boundary inversion algorithm to two synthetic MT data sets and one data set from an MT survey over the Gemini subsalt petroleum prospect in the Gulf of Mexico, and compare the resulting models to those obtained by smooth inversion methods.

INVERSION METHOD

Our procedure to solve for a model with the smoothest possible boundaries between layers with contrasting conductivity is similar to the Occam inversion method, first developed by Constable et al. (1987) to solve for a layered conductivity model fitting MT data at a single station. That is, we use a regularized inversion algorithm that minimizes some measure of model roughness under the constraint that the resulting response fits the data to an acceptable level of misfit. A Lagrange multiplier that controls the trade-off between the model roughness norm and the data misfit is varied at each iteration to find an optimal model. The application of the Occam inversion to solve for a smooth conductivity model in two dimensions is described in de Groot-Hedlin and Constable (1990). The main difference between the inversion algorithm described in that paper and the one outlined here is in the definition of the model roughness.

Here, we review the mathematical notation used in the Occam inversion and describe the modifications necessary to solve for models of the type shown in Figure 1. As shown, we represent the earth's subsurface in terms of a 2D model consisting of a limited number of layers of laterally varying thickness, each having uniform resistivity, over a half-space. The model is further split up into a grid of blocks, with boundary depths increasing exponentially to correspond with the loss of resolution with depth. Finally, the blocks are further subdivided into a finite-element grid for computation of responses and model sensitivities. Both the resistivities of each layer and the basal half-space, as well as the laterally variable layer depths, are allowed to vary within each inversion. However, layer depths can only take incremental values corresponding to the block boundaries. The model is set up such that the size of the blocks is smaller than the data resolution length, so that an upward or downward perturbation in depth to the nearest block boundary has little effect on the model response. Thus, for a model consisting of n_r layers over a half-space and n_c columns of blocks, the model is represented by a length $(n_r + 1) + n_r \times n_c$ vector **m** of parameters

$$[\log(\rho_1), \log(\rho_2), \ldots, \log(\rho_{n_r+1}),$$
$$\ln(d_{11}), \ldots, \ln(d_{1n_c}), \ldots, \ln(d_{n_r1}), \ldots, \ln(d_{n_rn_c})],$$

where ρ_i is the resistivity of the ith unit and d_{ij} is the depth of the bottom of the jth column of the ith layer. Resistivities are parameterized in terms of their logarithms since they can vary over several orders of magnitude. Depths are parameterized in terms of their natural logarithms since the block unit depths increase exponentially. A parameterization in terms of linear depth would result in greater roughness penalties applied to the deeper layers.

We define the roughness of the layers as

$$R = \|\mathbf{Sm}\|^2, \tag{1}$$

where **S** is a finite difference matrix that approximates a first-derivative operator. In the completely general case, we apply penalties both to differences in the resistivity between adjacent layers, and to lateral variation in layer depth. We suppress the boundary roughness to avoid spurious artifacts in the models. Ideally, we would not apply any penalty at all to the unit resistivities. However, MT responses become increasingly nonlinear as the resistivity contrast between adjacent layers increases, and the inverse problem becomes correspondingly nonlinear. Application of penalties on resistivity contrasts thus serves to stabilize the inversion. The general form for the model roughness operator is

$$\mathbf{S} = \begin{pmatrix} \mathbf{S}_{rho} & \mathbf{0} \\ \mathbf{0} & \mathbf{S}_{dep} \end{pmatrix}. \tag{2}$$

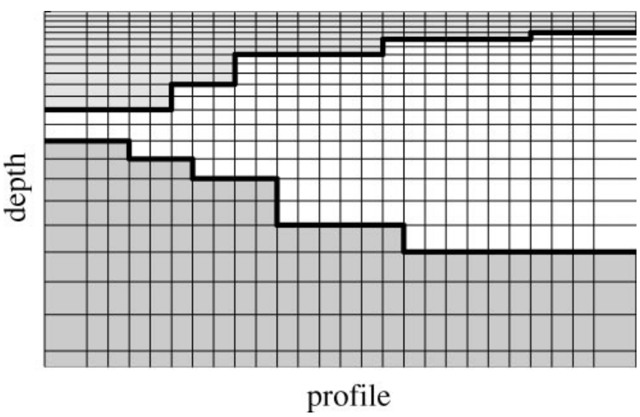

FIG. 1. Model setup. Each model consists of several layers with uniform resistivity but laterally varying thickness over a half-space. Each resistivity unit is further subdivided into a grid of blocks. Unit depths may only take on incremental values corresponding to block boundaries.

The $n_r \times (n_r + 1)$ matrix $\mathbf{S}_{rho}$ operates only on the resistivity parameters, and is defined by

$$\mathbf{S}_{rho} = \begin{pmatrix} c & -c & 0 & 0 & \dots \\ 0 & c & -c & 0 & \dots \\ & & \dots & & \\ & & \dots & c & -c \end{pmatrix}, \tag{3}$$

where c is a constant that controls the relative weighting between layer roughness and resistivity contrasts. The penalty matrix $\mathbf{S}_{dep}$ acts only on the depth parameters, and is given by

$$\mathbf{S}_{dep} = \begin{pmatrix} \mathbf{S}_1 & \mathbf{0} & \dots & & \\ \mathbf{0} & \mathbf{S}_2 & \mathbf{0} & \dots & \\ & \dots & & & \\ & \dots & \mathbf{0} & \mathbf{S}_{nr} & \end{pmatrix}, \tag{4}$$

where $\mathbf{0}$ is an $(n_c - 1) \times n_c$ matrix of zeros and $\mathbf{S}_i$ is the $(n_c - 1) \times n_c$ roughening matrix for the bottom of the ith layer, i.e.,

$$\mathbf{S}_i = \begin{pmatrix} 1 & -1 & 0 & \dots & & \\ 0 & 1 & -1 & 0 & \dots & \\ & \dots & & & & \\ \dots & & 0 & 1 & -1 & \end{pmatrix}. \tag{5}$$

Thus $\mathbf{S}_i$ differences the model depth parameters between laterally adjacent columns in layer i.

We simultaneously minimize model roughness and data misfit by finding a stationary point for the functional

$$U = \|\mathbf{Sm}\|^2 + \mu^{-1}\left[\|\mathbf{W}(\mathbf{d} - F[\mathbf{m}])\|^2 - \chi_*^2\right]. \tag{6}$$

The trade-off between the data misfit, given by the second term, and the model roughness is controlled by the Lagrange multiplier μ^{-1}. In equation (6), $\mathbf{d}$ represents the magnetotelluric data, $F[\mathbf{m}]$ is a nonlinear forward functional F acting upon the model $\mathbf{m}$ to produce the model response, χ_*^2 is the desired level of fit, and $\mathbf{W}$ is a diagonal matrix with entries inversely proportional to the data errors.

Since the forward functional $F[\mathbf{m}]$ is nonlinear with respect to perturbations in resistivity or boundary depth, we linearize about a starting model $\mathbf{m}_i$. The first two terms of the Taylor approximation yield

$$F[\mathbf{m}_i + \Delta\mathbf{m}] = F[\mathbf{m}_i] + \mathbf{J}_i \Delta\mathbf{m}, \tag{7}$$

where $\mathbf{J}_i$ is the Jacobian matrix of partial derivatives of $F[\mathbf{m}_i]$ with respect to the model parameters. The stability of any linearized inversion method is controlled largely by the accuracy of this approximation. In MT, equation (7) is a good approximation for models with limited conductivity contrasts; thus, linearized inversion methods tend to be highly robust for inversions that limit conductivity variability. With the large conductivity contrasts that are characteristic of inversions for boundary locations, this approximation becomes less accurate, and the iterations may reach local, rather than global, minima in the solution space. In the next two sections, we discuss methods to avoid converging to a local minimum.

We use the 2D finite element code of Wannamaker et al. (1987) to derive forward responses, and the adjoint method, described in deLugao and Wannamaker (1996), to compute partial derivatives of $F[\mathbf{m}_i]$ with respect to conductivity. Use of the adjoint method allows us to obtain the model sensitivities with respect to conductivity at minimal computational cost. To take advantage of the computational time saving offered by use of the adjoint method, we use a chain rule method to convert derivatives with respect to conductivity to derivatives with respect to depth. This is described in greater detail in the Appendix.

As derived in Constable et al. (1987), the model $\mathbf{m}_{i+1}$ is given by the stationary points of U, i.e.,

$$\mathbf{m}_{i+1} = \left[\mu(\mathbf{S}^T\mathbf{S}) + (\mathbf{WJ}_i)^T(\mathbf{WJ}_i)\right]^{-1}(\mathbf{WJ}_i)^T\mathbf{W}\hat{\mathbf{d}}_i, \tag{8}$$

where $\hat{\mathbf{d}}_i$ is given by $\mathbf{d} - F[\mathbf{m}_i] + \mathbf{J}_i\mathbf{m}_i$. Note that we need $\mathbf{S}^T\mathbf{S}$, not $\mathbf{S}$ itself. We use sparse matrix multiplication to compute $\mathbf{S}^T\mathbf{S}$ efficiently. Boundary depths computed from equation (8) are adjusted to the value of the nearest block boundary, as indicated in Figure 1, prior to computation of the forward response. Given that model sensitivities with respect to depth are much smaller than the derivatives with respect to unit conductivity, this does not significantly alter the model responses. At each iteration, we vary μ to find the model which generates the minimum misfit, and use this model as the starting point in the next iteration. If the misfit is less than χ_*, we increase μ to find smoother models until the desired misfit is attained.

Unlike for the Occam method (de Groot-Hedlin and Constable, 1990), the starting model for this algorithm must possess some resistivity contrasts. One reason is that our method of computing derivatives with respect to resistivity (described in the Appendix) requires that some conductivity contrast is present in adjacent units. Another reason is that we initialize boundary depths in terms of where conductivity contrasts exist in the initial model. For subsequent inversions, intermediate model solutions that feature very low resistivity contrasts between adjacent layers can also yield instability in the algorithm, since the model response is insensitve to perturbations in the boundary depth between two adjacent units with almost identical resistivity. In this case, the two units can be merged into one for further iterations. Also note that, because boundaries are parameterized in terms of the logarithm of the depth rather than thickness, the solution of equation (8) allows layer boundaries to cross over. When this occurs, we set the depth of the "lower" boundary equal to that of the "upper" boundary, thus pinching out a portion of the intermediate layer. Layers that are completely pinched out in an inversion must be removed for further iterations to maintain stability.

In application, we found that the algorithm converged slowly unless we chose a fairly good starting model. One option, used in the real data example, is to find the best layered model fitting the data with a 1D inversion algorithm, and use this layered solution as a starting model for the 2D algorithm. Another option is to use results from the smooth Occam method to build a starting model. We note that different starting models may yield different model solutions, especially when solving for a model with many layers. We attribute this to the inherent nonlinearity of the MT problem in the presence of sharp resistivity contrasts; the solution space of a nonlinear problem may possess many local minima in which a linearized algorithm may become trapped. The inversion algorithm is terminated when the inversion models show little variation after several iterations.

SYNTHETIC TESTS

We test the algorithm on two models of the type shown in Figure 2, with resistivity values of each model listed in Table 1. Model A features a conductive wedge underlying a highly resistive surface layer and overlying a basement of intermediate resistivity, representative of sediments below basalts. The second model (B) represents a resistive wedge-shaped body within a more conductive matrix, typical of salt structures found in the Gulf of Mexico. For each model, apparent resistivity and phase data for both the transverse electric (TE) and transverse magnetic (TM) modes were generated at 21 stations, spaced at 0.5-km intervals. The frequency ranges were chosen such that the penetration depth corresponds to the top unit at the highest frequency and to the bottom unit at the lowest frequency. Responses were computed at five frequencies per decade (i.e., at 24 frequencies from 400 to 0.01 Hz for the model featuring the conductive wedge, and for 20 frequencies from 4 to 0.0063 Hz for the resistive wedge model). To simulate noisy data, 5% random Gaussian noise was added to the resistivity and 1.4° to phase data prior to inversion. Since data errors are Gaussian distributed, and the diagonals of **W** are the reciprocals of standard deviations in the apparent resistivity and phase, the desired level of misfit is rms 1.0.

For each inversion, the models were represented by a grid of 68 columns and 36 rows of blocks. Although the 5.7° slope at the upper boundary of the wedge and the 16.6° slope at the lower boundary were modeled precisely using triangles in the finite-element formulation of the forward modeling algorithm, the inversion procedure only allows for slopes to be modeled using a stairstep approximation. Furthermore, the grid used for the inversion is not the same one used for the forward computations; that is, the grid we used does not allow depth values to be assigned their "true" values used in the synthetic model. This provides a realistic test of the algorithm as the locations of conductive boundaries are rarely known in advance. We computed responses for models discretized on this grid that most closely resemble the starting models of Figure 2 and Table 1 to determine the effect of gridding on the data misfit. We found that the rms misfit for the gridded model was 1.55 for the conductive wedge model and 1.5 for the resistive wedge model; thus, a finer grid discretization would be needed to represent the model more accurately. However, note that these are not necessarily the best-fitting models for this level of discretization, as resistivities and boundary depths can be adjusted slightly in order to yield a model that fits the data slightly better.

The number of discrete resistivity units must be specified in the starting model. We used a three-layer starting model for each inversion of the synthetic data, with resistivities and depths as listed in Table 2. The boundary depth values for the starting model were set by dividing the model into three layers, each consisting of 12 rows of blocks; initial resistivities were based on values shown in the relevant pseudosections of the apparent resistivity data.

Table 1. Synthetic model resistivities (in ohm-meters).

Unit number	Model A	Model B
1	1000	1
2	10	100
3	100	1

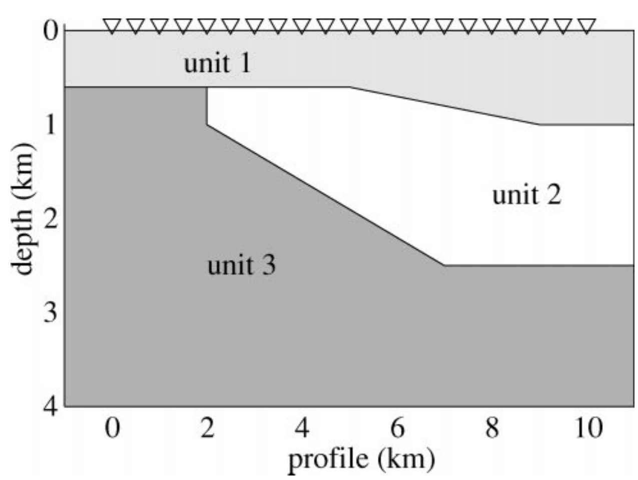

FIG. 2. The 2D resistivity model for the inversions of synthetic data, shown at 2:1 vertical exaggeration. The model features two sloping boundaries and a blunt termination for the middle layer. Unit resistivities are given in Table 1. Triangles indicate station locations.

Model A: Conductive wedge

The noisy synthetic data for model A are shown in pseudosection in Figure 3. The data were inverted with no penalty on

Table 2. Starting model for each inversion.

Boundary depth (km)	Model A (ohm-m)	Model B (ohm-m)
1.102	631	1.3
2.590	31.6	3.2
half-space	63.1	1.6

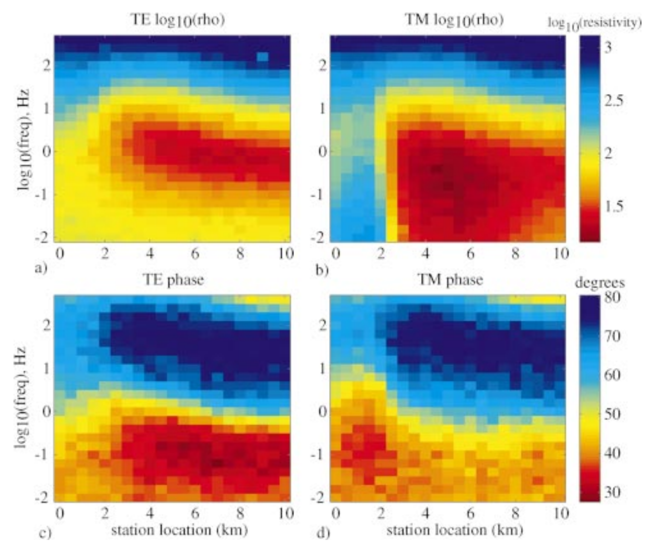

FIG. 3. Pseudosections of the responses of model A, which features a conductive wedge. (a) TE apparent resistivities $log_{10}(\rho_a)$. (b) TM apparent resistivities $log_{10}(\rho_a)$. (c) TE phase responses. (d) TM phase responses.

the differences in resistivity (i.e., only lateral variability in layer depths were penalized). The best-fitting model achieved by this inversion was attained after 13 iterations and has an rms misfit of 1.26. Comparison of the solution (shown in Figure 4) with the original wedge shape shown superimposed on the model, indicates that both the unit conductivities and boundary locations have been well imaged. In particular, the shape of both the top and bottom wedge boundaries are well recovered within the limits afforded by the stairstep approximation. However, instead of a blunt termination of the wedge to the left, the recovered conductor pinches out gradually, and several isolated conductors appear to the left of where the wedge termination should occur. These artifacts result from the smoothing constraints forced on the layer-depth parameters, and indicate that blunt terminations may be poorly imaged by this method.

Comparison of the synthetic data and model responses indicates that the fit is poorest for the five stations at the left end of the model. The poor fit at these stations is due to the the presence of the isolated conductors there, which result from the smoothing constraint on the layer boundaries. The adequate fit at the remainder of the stations suggests that sloping boundaries are adequately represented by the stairstep approximation.

For comparison, we inverted these data using the Occam 2D MT algorithm (de Groot-Hedlin and Constable, 1990), which solves for the smoothest possible model (Figure 5). Again, we represented the model by a grid of 68 columns and 36 rows. We specified an rms misft equal to that achieved by the boundary layer inversion. We note that much lower misfits could have been achieved by the smooth inversion method, because there are (68×36) free parameters using this method, while the boundary layer inversion has only $(3 + 68 \times 2)$ degrees of freedom. The solution to this inversion was attained after six iterations. The shape of the wedge is reproduced quite well, but the resistivities are less well recovered. Also, it is not clear where one would choose to place the lower boundary of the wedge structure.

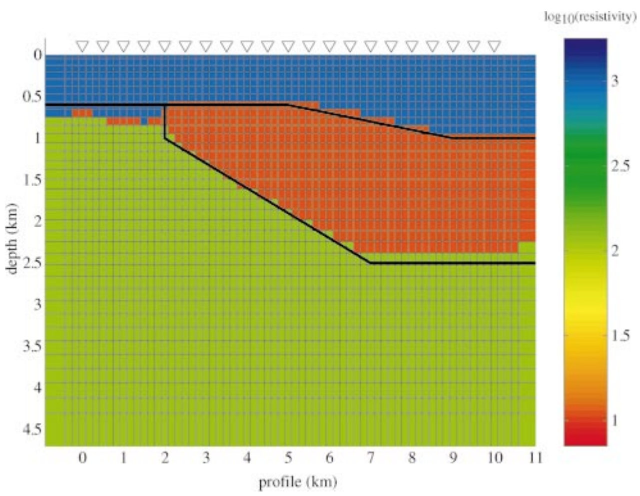

FIG. 4. Model recovered from boundary location inversion of data shown in Figure 3. The model is shown at 2:1 vertical exaggeration. The wedge boundaries are shown superimposed on the model. The station locations are indicated by the triangles at the top of the profile.

Model B: Resistive wedge

The noisy synthetic data for model B are shown in pseudosection in Figure 6. The model response is much weaker for this model than for model A, which is expected as the MT method is less sensitive to resistive anomalies than to conductive anomalies. Again, the data were inverted with no penalty on the resistivities, with the starting model listed in Table 2. The true model was poorly recovered in a straightforward application of the boundary location inversion to these synthetic data (i.e., although the final misfit was only 1.19, the solution was unrealistically rough). Relaxing the target misfit to 1.25 still resulted in an overly rough model, suggesting that the inversion achieved a local, rather than global, minimum. We attribute this to the

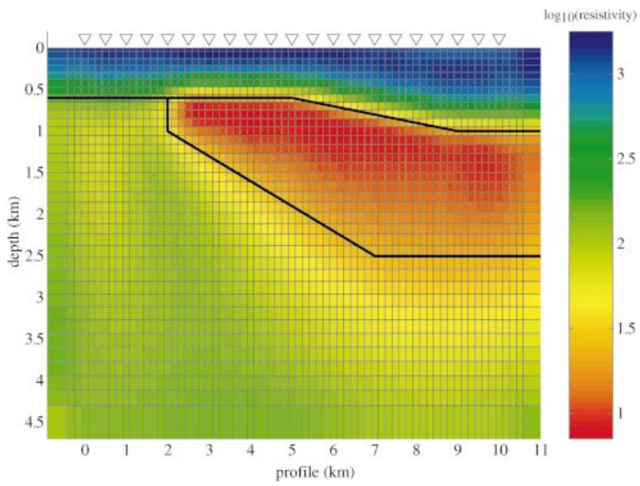

FIG. 5. Model recovered from smooth inversion of data shown in Figure 3. The model is shown at 2:1 vertical exaggeration. The wedge boundaries are shown superimposed on the model. The station locations are indicated by the triangles at the top of the profile.

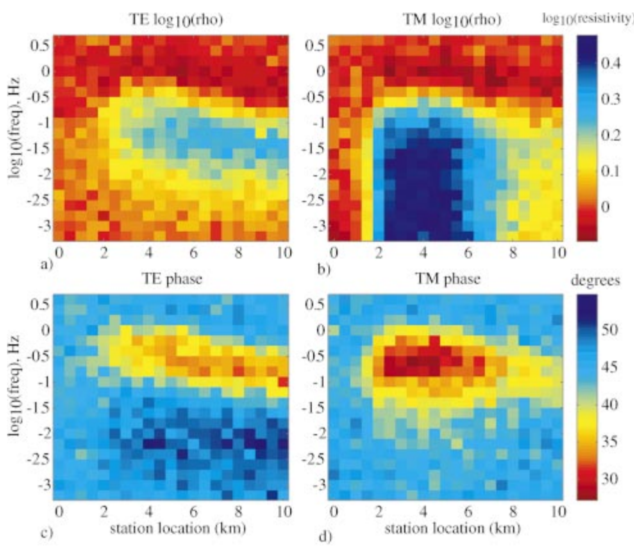

FIG. 6. Pseudosections of the responses of model B, which features a resistive wedge. (a) TE apparent resistivities $log_{10}(\rho_a)$. (b) TM apparent resistivities $log_{10}(\rho_a)$. (c) TE phase responses. (d) TM phase responses.

fact that the inverse problem becomes increasingly nonlinear with increasing roughness; thus, the Jacobian sensitivities are an inaccurate estimate of the gradient in the solution space.

To obtain a better model, we split the inversion into several steps in which we sequentially lower the target χ^2. At each step, we reach the target misfit and perform several more iterations to smooth the model further. This ensures that the starting model at each iteration is reasonably smooth, so that a globally smooth model can be found. The best smoothed model we could achieve has an rms misfit of of 1.15 and was reached after a total of 22 iterations.

This model, shown in Figure 7, shows that both the resistivities and boundary locations are reasonably well recovered; the resistivity of the wedge is 74 ohm-m in this model, and the overlying and underlying layers each have a resistivity of 1 ohm-m. The blunt termination of the wedge at the left is accurately imaged, but the flattening out of the wedge at the right is poorly imaged. Indeed, the data residuals indicate that the fit is poorest for the stations at the right.

We applied the Occam inversion method to these data, with a target rms of 1.15; the model shown in Figure 8 was attained after nine iterations. Obviously, this model does not resemble the model recovered from the boundary inversion method, although the response yields an equal misfit to the data. This is symptomatic of the nonuniqueness inherent in the MT method. The fact that highly dissimilar models can yield equivalent responses indicates that the model solution is highly dependent on the choice of norm imposed on the model within the regularization procedure. It also indicates the importance of a reasonable choice of starting model for the sharp boundary inversion. Thus, application of geologically realistic constraints is particularly important for imaging resistive targets using the MT method.

INVERSION OF REAL DATA

A marine MT(MMT) survey was carried out in the Gulf of Mexico in 1997 to test the feasibility of using sea-floor MT data to image the base of salt structures (Constable et al., 1998; Hoversten et al., 2000). Imaging these structures is of interest to the petroleum industry as salt structures are associated with hydrocarbon traps. The high acoustic contrast between salt bodies and the surrounding matrix makes it difficult and costly to image the shape of these bodies seismically. On the other hand, the high resistivity contrast between salt bodies and the surrounding water-saturated sediments (salt bodies are highly resistive) makes it a good target for MMT exploration.

The 1997 MMT survey was conducted over the Gemini subsalt petroleum prospect located at 28°46′N, 88°36′W. Its shape was previously determined using 3D seismic prestack depth migration, along with depth constraints provided by well logs. In this section, we use the boundary inversion method to examine whether MMT data can be used to independently constrain the shape of a salt body. Bathymetry along the transect considered here is minor; there is less than 200-m relief along the line. Furthermore, the skin depths in the conductive sea-floor sediments are small, so field distortions due to bathymetric variations are quickly dissipated. Therefore, bathymetric corrections may be neglected in the following analysis.

The Gemini salt structure is a 3D body; thus, the electric and magnetic fields do not decouple into two modes, as they would for an ideal prism. The survey line was along a perpendicular to a subsection of this structure that is 3–4 times longer than it is wide, approximately along its middle. TM mode impedances were calculated using the electric (**E**) field perpendicular to the long axis of the body (local strike) and magnetic (**H**) field parallel to the strike. Previous numerical modeling studies (e.g., Wannamaker et al., 1984) show that the response for a centrally located profile across an elongate 3D body agrees with the TM response for a 2D body with identical cross-section. Thus, we invert the TM mode data to image the cross-section of the 3D body. The TM data, shown at left in Figure 9, are relatively noisy. Error estimates for the apparent resistivities and phases are as high as 50%; the minimum error is taken to be 10%. Data from 15 sites at an average spacing of 0.9 km are considered.

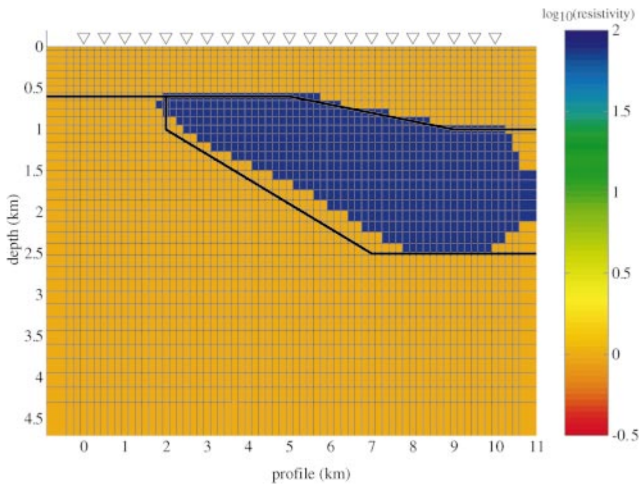

FIG. 7. Model recovered from boundary location inversion of data shown in Figure 6. The model is shown at 2:1 vertical exaggeration. The wedge boundaries are shown superimposed on the model. The station locations are indicated by the triangles at the top of the profile.

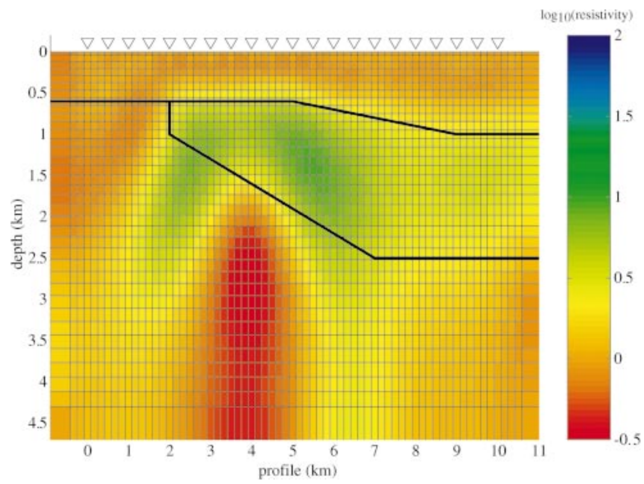

FIG. 8. Model recovered from smooth inversion of data shown in Figure 6. The model is shown at 2:1 vertical exaggeration. The wedge boundaries are shown superimposed on the model. The station locations are indicated by the triangles at the top of the profile.

We started the inversion of these data with a best-fitting seven-layer model determined from a 1D inversion of the data. The resistivities and depths with respect to the sea floor as listed in Table 3. For the first several iterations, no penalty was applied to resistivity contrasts between layers. A single layer was pinched out in the first iteration and the inversion was restarted with six units. After several iterations, the models feature large conductivity contrasts between units, and the algorithm converges poorly due to breakdowns in the linear approximations. Therefore, the inversion was restarted with a small penalty applied to differences between the resistivities of adjacent units [i.e., the value c in equation (3) is given a small nonzero value].

The final model, attained after a total of 18 iterations has an rms misfit of 1.2 and is shown in Figure 10. The shape of the body determined by 3D seismic prestack migration is shown superimposed. The model results indicate that the shape of the lower salt boundary is quite well resolved. Further tests with other starting models confirmed that the shape of the salt structure is consistently recovered in the inversion for boundary depths; however, the resistivity of this structure is less well resolved. The salt resistivities recovered ranged from 10 to 100 ohm-m. The TM mode response of the model in Figure 10 is shown at right in Figure 9. Comparison with the original data indicates that the broad features of this noisy data set are reproduced; the resistive salt body is manifested as a "pull-up" of the low resistivities in the middle of the TM resistivity data, and as an isolated region of low values in the phase data. Thin resistive layers at 1 km below the sea floor to the northeast of the salt body are not represented in the seismic model, but have been confirmed by controlled source EM sounding.

For comparison, we inverted these data using the Occam inversion, with a target misfit of 1.2. The algorithm converged to the model shown in Figure 11 in three iterations. The top of the salt structure is reasonably well resolved by this smooth inversion method, but the bottom is very poorly resolved although the residuals indicate that the broad features of the data are adequately recovered. These results indicate that a contrast in resistivities at the top of the salt boundary is required by the data, but that little contrast is required at the bottom boundary at this misfit level. However, the existence of a sharp

Table 3. Starting model for inverting Gemini data.

Boundary depth (km)	Resistivity (ohm-m)
0.446	0.73
1.023	1.23
1.918	1.25
3.298	1.47
5.424	1.16
8.704	3.89
half-space	5.96

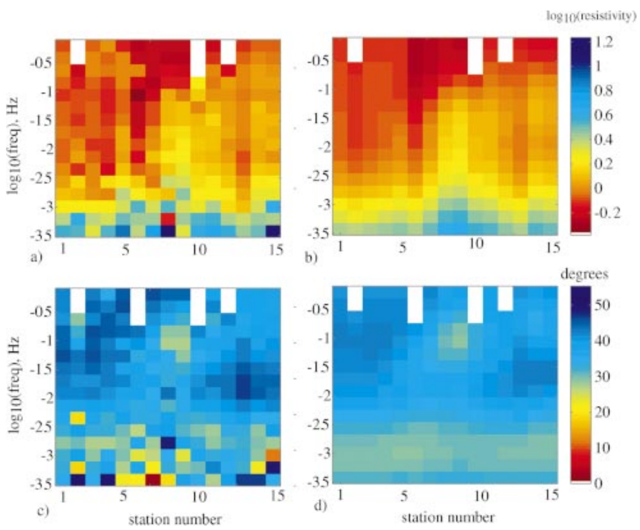

FIG. 9. Gemini data. (a) TM mode $\log_{10}(\rho_a)$ data. (b) Pseudosection of the response of the model shown in Figure 10 $log_{10}(\rho_a)$. (c) TM mode phase data. (d) Pseudosection of the TM phase response of the model shown in Figure 10.

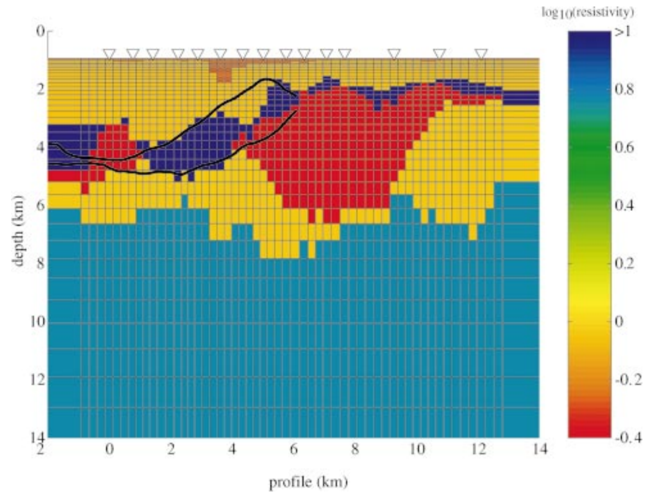

FIG. 10. Model recovered from boundary location inversion of the Gemini data. The shape of the salt body recovered from 3D seismic prestack migration is shown superimposed on the model. Station locations are indicated by the triangles at the top of the profile. The station locations are indicated by the triangles at the top of the profile.

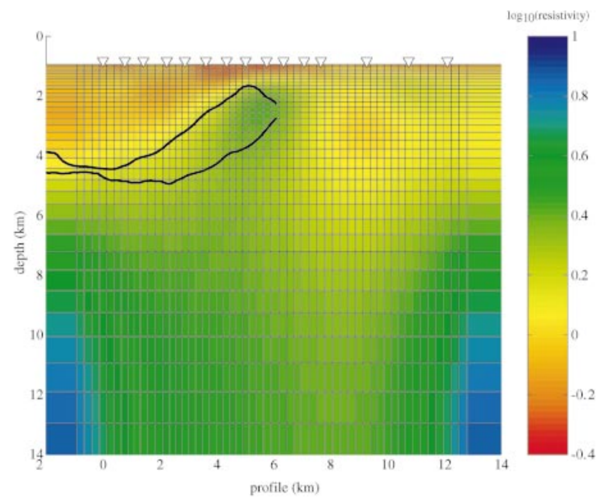

FIG. 11. Model recovered from Occam inversion of Gemini data. The station locations are indicated by the triangles at the top of the profile.

conductivity contrast at the bottom boundary is a reasonable geological constraint. Thus, given the geological constraint that the subsurface consists of regions with sharp resistivity contrasts, the inversion for boundary depths yields the most realistic model that fits the data at a given misft level. (Note that the bottom boundary can be recovered by the smooth Occam routine by decreasing the misfit, but in this paper we want to compare models with similar misfits.)

DISCUSSION AND CONCLUSIONS

Given that there are a multiplicity of resistivity structures that can fit a noisy MT data set equally well, the choice of MT inversion method should be guided by the type of subsurface structure present. For instance, some smooth inversion methods, such as the Occam method used in the examples, do not discriminate between vertical and horizontal structure, and are thus useful in regions where little is known a priori about the subsurface. The boundary inversion method described here favors layered structures with possibly large conductivity contrasts between adjacent layers, and is useful where the geological formations are relatively flat lying.

For structures that are very well resolved by the data, like the conductive wedge, there is little difference in the features of the final models obtained using the Occam method and the boundary inversion method. However, a sharp boundary inversion allows depths of interfaces to be found directly without interpreting gradients in resistivity. For structures that are poorly resolved by the data, like the resistive wedge, the type of regularization has a much greater impact on the final model. Thus, the boundary inversion method is a good choice if the target anomaly is known to be resistive and to have a strong conductivity contrast with the surrounding medium.

Due to inaccuracy of the linear approximation in the presence of strong conductivity contrasts, the boundary inversion method can be unstable, and somewhat prone to finding local minima. One solution, used in the application of this method to the Gemini data set, is to apply a small penalty to the differences in resistivity between adjacent layers. This prevents the contrast from becoming large in the initial iterations, so that the linear approximation remains sufficiently accurate. Another approach, demonstrated in the resistive wedge example, is to apply the boundary inversion method in several steps so that we find the smoothest model at a particular misfit at each step. In this way, the algorithm's search is directed toward models with smooth boundaries.

ACKNOWLEDGMENTS

We thank Kerry Key for processing the Gemini data and discussions on its analysis, David Bartel of Chevron Texaco for providing us the shape of the Gemini salt volume as determined by seismic data, and Phil Wannamaker for providing us with the adjoint method of solving for Jacobian sensitivities, which sped up the inversion algorithm considerably. We are also grateful to Pamela Lezaeta, Colin Farquharson, and an anonymous reviewer for careful reviews. This work was supported by the Scripps Seafloor Electromagnetic Methods Consortium.

REFERENCES

Constable, S. C., Parker, R. L., and Constable, C. G., 1987, Occam's inversion: A practical algorithm for generating smooth models from EM sounding data: Geophysics, **52**, 289–300.

Constable, S. C., Orange, A., Hoversten, G. M., and Morrison, H. F., 1998, Marine magnetotellurics for petroleum exploration, Part 1: A sea-floor equipment system: Geophysics, **63**, 816–825.

de Groot-Hedlin, C., and Constable, S., 1990, Occam's inversion to generate smooth, two-dimensional models from magnetotelluric data: Geophysics, **55**, 1613–1624.

de Lugao, P. P., and Wannamaker, P. E., 1996, Calculating the two-dimensional magnetotelluric Jacobian in finite elements using reciprocity: Geophysical Journal International, **127**, 806–810.

Gill, P. E., Murray, W., and Wright, M. H., 1981, Practical optimization: Academic Press.

Hoversten, G. M., Constable, S. C., and Morrison, H. F., 2000, Marine magnetotellurics for base-of-salt mapping: Gulf of Mexico field test at the Gemini structure: Geophysics, **65**, 1476–1488.

Jupp, D. L. B., and Vozoff, K., 1977, Two-dimensional magnetotelluric inversion: Geophysical Journal of the Royal Astronomical Society, **50**, 333–352.

Marcuello-Pascual, A., Kaikkonen, P., and Pous, J., 1992, 2-D Inversion of MT data with a variable model geometry: Geophysical Journal International, **110**, 297–304.

Mehanee, S., and Zhdanov, M., 2002, Two-dimensional magnetotelluric inversion of blocky geoelectrical structures: Journal of Geophysical Research, **107**, EPM1-11.

Oristaglio, M. L., and Worthington, M. H., 1980, Inversion of surface and borehole electromagnetic data for two-dimensional electrical conductivity models: Geophysical Prospecting, **28**, 633–657.

Rodi, W., 1989, Regularization and Backus-Gilbert estimation in nonlinear inverse problems: Applications to magnetotellurics and surface waves: Ph.D. dissertation, Pennsylvania State University.

Rodi, W., and Mackie, R. L., 2001, Nonlinear conjugate gradients algorithm for 2-D magnetotelluric inversion: Geophysics, **66**, 174–187.

Smith, T., Hoversten, M., Gasperikova, E., and Morrison, F., 1999, Sharp boundary inversion of 2D magnetotelluric data: Geophysical Prospecting, **47**, 469–486.

Smith, T., and Booker, J. R., 1991, Rapid inversion of two- and three-dimensional magnetotelluric data: Journal of Geophysical Research, **96**, 3905–3922.

Tihonov, A. N., 1963a, Regularization of incorrectly posed problems: Soviet Math. Dokl., **4**, 1035–1038.

——— 1963b, Solution of incorrectly formulated problems and the regularization method: Soviet Math. Dokl., **4**, 1624–1627.

Uchida, T., 1993, Smooth 2-D inversion for magnetotelluric data based on statistical criterion ABIC: Journal of Geomagnetism and Geoelectricity, **45**, 841–858.

Wannamaker, P. E., Hohmann, G. W., and Ward, S. H., 1984, Magnetotelluric responses of three-dimensional bodies in layered earths: Geophysics, **49**, 1517–1533.

Wannamaker, P. E., Stodt, J. A., and Rijo, L., 1987, A stable finite-element solution for two-dimensional magnetotelluric modeling: Geophysical Journal of the Royal Astronomical Society, **88**, 277–296.

APPENDIX A

COMPUTATION OF MODEL SENSITIVITIES

The finite element code for 2D MT modeling, described in Wannamaker et al. (1987), is used for computation of model responses, along with code to calculate Jacobian sensitivities, described by de Lugao and Wannamaker (1996). The model sensitivities are derived using an adjoint method, which allows the sensitivities to be obtained at minimal additional computational cost over that required for calculation of model responses.

The Jacobian terms output by this code provide partial derivatives of each datum with respect to small changes in model resistivities. It is simple to convert these quantities to Jacobian sensitivities with respect to $\log(\rho_i)$ by application of the chain rule, i.e.,

$$\frac{\partial(datum)}{\partial(\log(\rho_i))} = \frac{\partial(datum)}{\partial(\rho_i)} \times \frac{\partial(\rho_i)}{\partial(\log(\rho_i))} = \frac{\partial(datum)}{\partial(\rho_i)} \times 2.3026\rho_i, \qquad \text{(A-1)}$$

where ρ_i denotes the resistivity of the ith block. The partial derivatives for changes in data with respect to variations in the log(*resistivity*) of each large unit are derived by summing the Jacobian values of all small blocks within that large unit. These quantities are exact to within the accuracy of the finite element modeling code.

We also use the chain rule to derive the partial derivatives of the data with respect to small changes in boundary depth through application of the chain rule, i.e.,

$$\frac{\partial(datum)}{\partial(\ln(d_i))} = \frac{\partial(datum)}{\partial(\rho_i)} \times \frac{\partial(\rho_i)}{\partial(\ln(d_i))}, \qquad \text{(A-2)}$$

where d_i is the depth parameter of interest. Again, the first term on the right side is the model sensitivity derived from the adjoint code. The second term is computed using a finite-difference method, i.e., for a given boundary layer depth, we divide the differences in resistivity across the boundary by the difference in ln($depth$). Given that derivatives are accurate only for small incremental variations, we are introducing some error into the data sensitivities with respect to depth, especially if either the resistivity contrast or the depth increments are large.

It is well known that the accuracy of a central finite-difference scheme is accurate to second order, whereas the accuracy of forward-difference or backward-difference approximations are accurate only to first order (e.g., Gill et al., 1981). Therefore, we compute data sensitivities with respect to depth using

$$\frac{\partial(datum)}{\partial(\ln(d_i))} = \frac{1}{2}\left(\mathbf{J}^{+}\frac{\partial(\rho)}{\ln(d_{+}) - \ln(d_i)} + \mathbf{J}^{-}\frac{\partial(\rho)}{\ln(d_{-}) - \ln(d_i)}\right), \qquad \text{(A-3)}$$

where d_i is the depth of boundary for a particular column within a layer and d_+ and d_- represent downward and upward increments in depth (depth increases downward), respectively. That is, d_+ is the depth of the bottom of the subunit just below the given boundary parameter, and d_- is the depth to the top of the subunit just above the given boundary parameter. The resistivity contrast between the units is given by $\partial(\rho)$, and $\mathbf{J}^+$ and $\mathbf{J}^-$ are the model sensitivities derived from the adjoint code for the model subunits below and above the given boundary parameter, respectively.